Applied Thermal Engineering 149 (2019) 1192–1202

Contents lists available at ScienceDirect

Applied Thermal Engineering

journal homepage: www.elsevier.com/locate/apthermeng

Research Paper

A novel one-dimensional model to predict fin efficiency of continuous fin-tube heat exchangers

Felipe Suárez[a], Sergio D. Keegan[b,c], Néstor J. Mariani[b,c], Guillermo F. Barreto[b,c,*]

[a] Departamento de Mecánica, Facultad de Ingeniería, UNLP, Argentina
[b] PROIRQ, Departamento de Ingeniería Química, Facultad de Ingeniería, UNLP, Argentina
[c] Centro de Investigación y Desarrollo en Ciencias Aplicadas "Dr. J. J. Ronco" (CINDECA), CONICET-UNLP-CIC BA, Argentina

HIGHLIGHTS

- A novel one-dimensional model to predict heat transfer from (or to) continuous fins and tubes was proposed.
- A wide range of tube pitches and operative conditions were tested.
- Remarkable agreement between numerical values and predictions is achieved.

ARTICLE INFO

Keywords:
Continuous fins
Fin efficiency
Fin-and-tube heat exchangers
One-dimensional model

ABSTRACT

The objective of this contribution is to present a novel one-dimensional (1D) model to predict the heat transfer rate from (or to) continuous fin-and-tube heat exchangers. In this model, called two equivalent radial fins (1D-TERF), it is proposed to represent the thermal behavior of the continuous two dimensional (2D) fin by employing two thermally independent sections of radial fins, while keeping the total surface area of the actual fin and the outer perimeter of the tube. The two geometrical free parameters of the model are obtained by matching the two first terms of the series describing the actual fin efficiency at low values of the modulus, $\Phi = \ell \sqrt{h/(k\ \delta)}$. It is demonstrated that the 1D-TERF model with this criterion allows estimating the fin efficiency with a higher level of precision than any other literature alternative (as the radial equivalent fin model and the sector method) over a wide range of conditions (*i.e.*, values of Φ between 0 and infinity) for circular tubes with in-line and staggered layouts in an extensive range of geometric ratios.

1. Introduction

Fin-and-tube heat exchangers are widely used in many applications such as cryogenic gas processing, aerospace devices, air conditioning and transport vehicles. Such a kind of heat exchangers presents high efficiency and multi-functionality [19,9].

Several aspects concerning the design and analysis of fin-and-tube heat exchangers have been undertaken in the open literature [7,25,33]. Specifically dealing with heat transfer in individual fin systems it is worth mentioning recent contributions of the groups of Professors Das and Kundu. The analysis of the transient behavior in pin and longitudinal wet fins is analysed in Wankhade et al. [30] and it is concluded that for an accurate analysis of a wet fin surface under transient heat conduction, a non-Fourier approach is most advisable. Also, a comparison between the results employing a Fourier and a non-Fourier approach for a novel configuration of longitudinal and pin fins attached to two surfaces under fully wet conditions was performed by Kundu et al. [16]. It is interesting to note that, despite the fact that steady state is the normal operating condition of heat exchanger devices in general and those having fins in particular, transient effects will arise during start-up and shut-down operations [1].

The effect of temperature on heat transfer parameters is studied in Singh et al. [27] for porous fins of stepped rectangular profile. Particularly concerning the thermal conductivity, an average value for metallic fins can be safely assumed, unless the temperature gradients along the fin length become very high. However, that situation will be accompanied by a low efficiency, improper of a correct design.

Optimization aspects can be found in Das and Kundu [6], in which, wet individual fins of concave parabolic and rectangular profiles are analyzed and it is proved that the former alternative provides more surface area and enhances the heat transfer rate for a given fin volume. It is also found that the influence of the fin thickness on heat transfer

* Corresponding author.
E-mail address: barreto@quimica.unlp.edu.ar (G.F. Barreto).

https://doi.org/10.1016/j.applthermaleng.2018.12.125
Received 3 October 2018; Received in revised form 20 December 2018; Accepted 23 December 2018
Available online 26 December 2018
1359-4311/

Nomenclature

A_T	surface area of the fin unit-cell [m^2]
P	arc length of the tube perimeter subtended by the unit cell ($\pi D/4$) [m]
D	tube diameter [m]
h	convective heat transfer coefficient [$W\,m^{-2}\,°C^{-1}$]
G	auxiliary field defined in Eq. (5a) [m^2]
I_n	first kind modified Bessel function of order n [–]
K_n	second kind modified Bessel function of order n [–]
k	thermal conductivity of the fin material, [$W\,m^{-1}\,°C^{-1}$]
m^2	parameter in Eq. (2c), $= h/k\,\delta$ [m^{-2}]
P_L	dimensionless longitudinal pitch = X_L/D [–]
P_T	dimensionless transversal pitch = X_T/D [–]
T	local fin surface temperature [K]
T_f	fluid temperature [K]
T_b	fin base temperature [K]
X_L	longitudinal pitch [m]
X_T	transversal pitch [m]
x, y	Cartesian coordinates
x^*, y^*	dimensionless Cartesian coordinates defined in Eqs. (2d) and (2e)

Symbols

δ	fin half-thickness [m]
Φ	modulus defined in Eq. (2c), $= \ell\sqrt{h/(k\,\delta)}$ [–]
ε	relative error defined in Eq. (17) [–]
γ	parameter defined in Eq. (4b) [–]
β	parameter defined in Eq. (4c) [–]
ℓ	effective length of conduction for the actual fin, $= A_T/P$ [m]
ℓ_R	effective length of conduction for a radial fin, $= (R_e^2 - R_i^2)/(2\,R_i)$ [m]
η	fin efficiency [-]
θ	dimensionless temperature defined in Eq. (2b) [–]

Subscripts and superscripts

1D-SERF	single equivalent radial fin model
1D-TERF	two equivalent radial fin model
SECT	sector method

rate is considerably higher than that of fin length and fin width.

Other relatively recent contributions are mainly focused on the mathematical treatment of the fin-efficiency problem. Campo and Delgado-Torres [2] developed an approximate analytical solution for annular fin efficiency transforming the modified Bessel equation of zero order into a Cauchy-Euler equation. Danish et al. [5] presents a close analytical solution for temperature profile and fin efficiency in a rectangular fin considering a power low variation for heat transfer coefficient and thermal conductivity while Sabbaghi et al. [24] present an analytical solution for the efficiency of a semi-spherical fin considering simultaneously heat and mass transfer.

The topic of fin efficiency estimation has been considerably less studied for the cases of continuous fin-and-tube configurations (*e.g.* [28,18,22,20]) and the literature is far from being comprehensive. Thus, the issue is still open to introduce new alternatives for predicting purposes.

From a general point of view, the thermal conduction phenomena in continuous fins of tubular heat transfer devices should be analyzed in two spatial directions (2D geometries), as temperature through the fin thickness can be considered to be uniform. In such cases a numerical solution of the energy conservation equation is required to obtain the heat transfer rate between the fin and the surrounding fluid or, in dimensionless terms, the fin efficiency [29,22,11,20,4]. Nowadays available numerical platforms allow readily performing the analysis of a single set of conditions or a limited number of them. However, if a recurrent simulation of the heat transfer unit is required, as in an optimization procedure, the heat transfer rate from the fins should be evaluated a very large number of times. Therefore, numerical procedures applied to two spatial directions may become highly impractical.

An appropriate approach to deal with the problem of estimating the efficiency in continuous fins is the use of one dimensional models (1D). To briefly describe these models, it is first recall that the tube bundle is arranged either in an in-line or staggered layouts with different transversal and longitudinal pitches, X_T and X_L, as sketched in Fig. 1a and Fig. 1b, where the shaded areas are the unit cells of the continuous fin to evaluate the heat transfer rate. The single equivalent radial fin model (1D-SERF) is one of the most widely employed approximations [31,14]. In the 1D-SERF model the unit cell is replaced by an annular circular sector of the same area and internal diameter equal to the tube diameter. By doing so, the efficiency of the actual fins can be estimated with a precision of around 5% for in-line layouts of tubes of circular cross section (see Fig. 1a) for longitudinal pitch/diameter ratios $2 \le P_L \le 4$ ($P_L = X_L/D$) and transversal/longitudinal pitch ratios $P_T/P_L \le 1.5$ ($P_L = X_L/D$). For staggered layouts (see Fig. 1b) within the same ranges of P_L and P_T/P_L, the relative errors using the 1D-SERF model are less than 1%. Nonetheless, for configurations outside the mentioned ranges the precision of the model is severely deteriorated (*e.g.*, for an in-line layout presenting $P_L = 2$ and $P_T/P_L = 2$ the relative

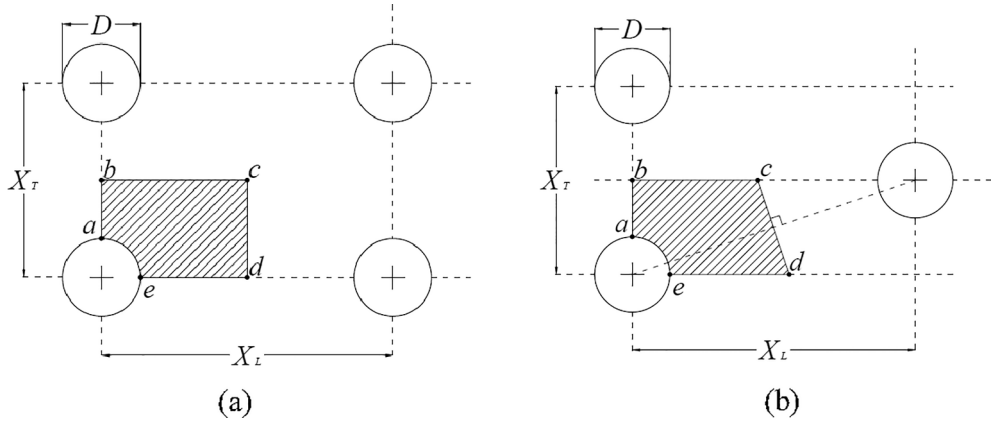

Fig. 1. Sketch of the continuous fin-and-tube layouts: (a) in-line, (b) staggered.

errors grow until approximately 10% and values greater that 30% arise for $P_T = 1.5$ and $P_T/P_L \geq 3.5$).

Another frequently recommended approximation to predict continuous-fin efficiency is the one known as sector method (SECT) [17,23,15]. The actual surface of the unit cell is divided into a number of coaxial sectors and each of them is replaced by an annular circular sector of the same area and internal diameter equal to the tube diameter. Each of these sectors is assumed to conduct heat independently of each other. The SECT method provides a better performance than the 1D-SERF for relatively small pitches (*e.g.*, $P_L \leq 2$), but not for larger values when (P_T/P_L) is relatively low (*e.g.*, for in-line layouts in the range $2 \leq P_L \leq 4$ with $P_T/P_L \leq 1.5$, both alternatives present similar errors).

In addition, typically the precision of the SECT and 1D-SERF approximations is reported in the literature for a single set of values of fin thermal conductivity, heat transfer coefficient and a fixed geometrical configuration or for a limited number of conditions. It seems more appropriate and relevant to perform an analysis for the complete set of possible conditions.

Therefore, it is desirable to have a highly accurate model that allows evaluating the fin efficiency of continuous fin-circular tubes systems for an extensive range of operative conditions and geometric ratios.

In this context, the purpose of this contribution is to present a novel one-dimensional model (1D), identified as 1D-TERF (Two Equivalent Radial Fins), to predict the fin efficiency of continuous fins in tubular heat exchangers. A uniform heat transfer coefficient (h) and fin thermal conductivity (k) under steady state conditions are considered according to the standard design procedures. The two geometrical parameters introduced by the 1D-TERF model are fitted by matching the thermal behavior of the actual fin at very low values of fluid/fin heat exchange rate as compared to heat conduction through the fin (*i.e.*, very low values of the modulus $\Phi = \ell\sqrt{h/(k\,\delta)}$). The comparison among the models will be performed by varying the pitches for in-line and staggered layouts of tubes of circular cross sections in an extensive range and covering the whole range of Φ. Finally, the direct use of a truncated series expansion of the fin efficiency in terms of Φ is analyzed.

2. Problem statement

Fig. 1a and Fig. 1b present the tube layouts for continuous fin-and-tube heat exchangers analyzed in this contribution. X_T and X_L in Fig. 1a and b are the transversal and longitudinal pitches, respectively, which are rendered dimensionless using the tube diameter, D (*i.e.*, $P_T = X_T/D$ and $P_L = X_L/D$). It is assumed that all the continuous fins and tubes behave identically from a thermal point of view. Thus, it is enough to analyze the shaded regions that define elementary unit cells. In Fig. 1a the straight segments hold adiabatic boundary conditions. The same happens for the segments a-b, b-c and e-d of Fig. 1b, but the segment c-d holds symmetric temperature and anti-symmetric heat fluxes with respect to the midpoint, and therefore the segment is globally adiabatic. In practice, the results are virtually the same if the segment c-d is regarded as being locally adiabatic, a conclusion that has been numerically checked and used in the formulation presented below.

The assumptions to formulate the energy balance for a continuous fin sketched in Fig. 1a and Fig. 1b are those usually adopted in the standard design procedure of recuperative heat exchangers in general and of continuous fin-and-tube units in particular [32,26]:

- Steady state operation
- Uniform thermal conductivity (k) and convective heat transfer coefficient (h)
- The fin half-thickness δ is small enough to disregard any variation of temperature along it (*i.e.*, in the normal direction to the plane containing Fig. 1a and Fig. 1b).
- No internal heat source.
- Negligible radiant effects.

$$k\left[\frac{\partial^2 T}{\partial x^2} + \frac{\partial^2 T}{\partial y^2}\right] = \frac{h}{\delta}(T - T_f) \tag{1}$$

No phase-change in the fluid stream was considered in Eq. (1). However, the analysis can be extended to air cooling operations in which dehumidification (*i.e.*, condensation) takes place in the whole fin provided that the Le (Lewis number) ~1 is assumed, according to the Chilton-Colburn analogy and adopting a linear relationship between the saturated humidity along the fin surface and the fin temperature [8,21]. In addition, for gaseous streams carrying particulate matter it is likely that the accumulation of deposits grows with time causing an additional thermal resistance [10]. The effect can be taken into account by a fouling factor and an effective heat transfer coefficient rather than the true convective heat transfer should be employed in Eq. (1).

Eq. (1) is rendered dimensionless as follows:

$$\frac{\partial^2 \theta}{\partial x^{*2}} + \frac{\partial^2 \theta}{\partial y^{*2}} - \Phi^2\,\theta = 0 \tag{2a}$$

$$\theta = \frac{T - T_f}{T_b - T_f}; \tag{2b}$$

$$\Phi^2 = m^2\ell^2 \tag{2c}$$

$$y^* = \frac{y}{\ell}; \tag{2d}$$

$$x^* = \frac{x}{\ell} \tag{2e}$$

In Eqs. (2) $\ell = A_T/P$ is the characteristic or effective length for thermal conduction, where A_T is the surface area of the elementary unit cell (*i.e.*, the shaded regions in Fig. 1a and b) and P is the arc length $\widehat{ea}$ in Fig. 1a and b. The tube temperature T_b in Eq. (2b) is assumed to be uniform along the perimeter. Eq. (2c) defines the modulus Φ while $m^2 = h/k\,\delta$.

The boundary conditions for Eq. (2a) are:

$$\theta = 1; \quad \text{on} \quad \widehat{ea} \text{ in Figs. 1a and b} \tag{2f}$$

$$\nabla_n\theta = 0; \quad \text{on} \quad a\bar{b}cde \text{ in Figs. 1a and b} \tag{2g}$$

Fin efficiency is defined as the ratio between the actual heat transfer rate and the maximum value that can be achieved (*i.e.*, the one that takes place if the whole fin presents the same temperature as the tube perimeter):

$$\eta = \frac{\iint_{A_T} \theta\, dx\, dy}{A_T} \tag{3}$$

2.1. Thermal behavior of a fin for high values of thermal conductivity

The fin efficiency can be expressed as a series from a regular perturbation analysis of Eq. (2) on Φ^2, regarded as a small parameter, as follows

$$\eta_{high} = 1 - \gamma\,\Phi^2 + \beta\,\Phi^4 \tag{4a}$$

where γ and β are expressed as:

$$\gamma = \frac{\iint_{A_T} G\, dx\, dy}{\ell^2 A_T} \tag{4b}$$

$$\beta = \frac{\iint_{A_T} G^2\, dx\, dy}{\ell^4 A_T}, \tag{4c}$$

G is an auxiliary field defined as:

$$\frac{\partial^2 G}{\partial x^2} + \frac{\partial^2 G}{\partial y^2} = -1 \quad on \quad A_T \tag{5a}$$

$$G = 0; \quad \text{on} \quad \widehat{ea} \text{ in Figs. 1a, b} \tag{5b}$$

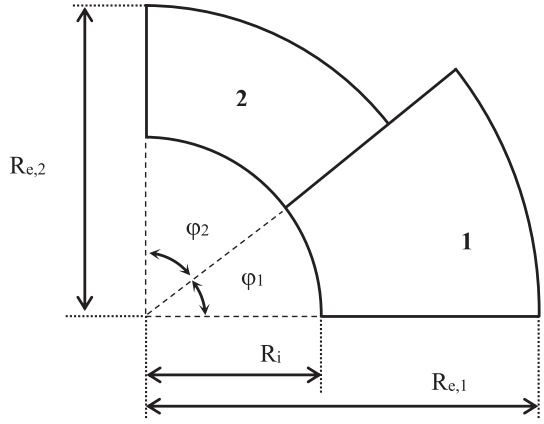

Fig. 2. Sketch of two equivalent radial fins (1D-TERF) model.

$$\nabla_n G = 0; \quad \text{on} \quad ab\bar{c}de \text{ in Figs. 1a, b} \tag{5c}$$

The detailed procedure for the perturbation analysis is included in Appendix A.

It is important to remark that parameters γ and β only depend on geometric features (*i.e.*, tube bundle layout and dimensionless transversal and longitudinal pitches, P_T and P_L). Thus, for a given geometry of the tube bundle, the solution of Eqs. (5) for G should be obtained once for all, regardless of the actual value of parameter Φ. The Comsol Multiphysics® platform is quite appropriate for this purpose, requiring a running time of a few seconds to achieve a precision of at least 0.1%.

Values of the parameters γ and β for staggered and in-line layouts and a large range of both dimensionless pitches, covering most cases likely to be found in practice, are included in Tables B1–4 of the Appendix B.

2.2. Thermal behavior of a fin for low values of thermal conductivity

For high values of the modulus Φ, it is also possible to carry out a perturbation analysis on 1/Φ to obtain a series solution for η, as was shown by the analogous process of diffusion and (isothermal first order) reaction in catalytic pellets [12]. By truncating the series up to the second order term, the following expression arises

$$\eta_{low} = \frac{1}{\Phi} + \frac{\ell}{D}\left(\frac{1}{\Phi}\right)^2 \tag{6}$$

Although the range of η values at which Eq. (6) will be suitable is not often found in actual fin design, the accuracy of any approximation intended to evaluate η will be enhanced if the Eq. (6) is satisfied for high enough values of Φ. In this regards, it is worth mentioning that all the approximate methods described in Section 3 below fulfill the limiting expression (6).

3. Fin efficiency estimation

The energy balance for a radial fin with uniform half-thickness (δ), internal and external radii, $R_i = D/2$ and R_e, respectively, can be written as follows:

$$\frac{d^2\theta}{dr^2} + \frac{1}{r}\frac{d\theta}{dr} - m^2\,\theta = 0 \tag{7a}$$

where θ and m are defined according to Eqs. (2).

Boundary conditions for Eq. (7a) are:

$$\theta = 1 \text{ at } r = R_i; \tag{7b}$$

$$d\theta/dr = 0 \text{ at } r = R_e \tag{7c}$$

The solution of Eqs. (7) can be retrieved from many textbooks (*e.g.*, [13]) and the fin efficiency can be expressed as:

$$\eta_R = \frac{1}{\Phi_R}\left[\frac{I_1(mR_e)\,K_1(mR_i) - K_1(mR_e)\,I_1(mR_i)}{K_1(mR_e)\,I_0(mR_i) + I_1(mR_e)\,K_0(mR_i)}\right] \tag{8}$$

where: $\Phi_R = m\,\ell_R$ with $\ell_R = m\,(R_e^2 - R_i^2)/(2\,R_i)$

Additionally, I_0, I_1, K_0 and K_1 are modified Bessel functions of the first (I) and second (K) type and integer order 0 and 1.

3.1. Single equivalent radial fin model (1D-SERF)

In the 1D-SERF model the actual unit cell is replaced by an annular circular sector of internal radius $R_i = D/2$ and external radius R_e defined to match the same surface-area of the actual unit cell such

$$R_e = \sqrt{4\frac{A_T}{\pi} + (D/2)^2} \tag{9}$$

Eq. (8) is then employed to calculate the fin efficiency when using the 1D-SERF model.

It is worth mentioning that Zabronski [31] provided a close solution to evaluate the fin efficiency of continuous fins with an in-line layout and $P_L = P_T$. He also shown that such a solution leads to similar values to those obtained using the 1D-SERF model. Some years later, Kuan et al. [14] extended the 1D-SERF model to continuous fins presenting other tube shapes (*i.e.*, different from the usual circular tubes).

3.2. Two equivalent radial fins model (1D-TERF)

A sketch of the "two equivalent radial fins" (1D-TERF) model is shown in Fig. 2. This model can be considered as an extension of the 1D-SERF model, but the single annular sector of the 1D-SERF model is split into two sectors of angles φ_1 and φ_2, each of them exchanging heat with the tube independently of each other (*i.e.*, the common boundary is adiabatic).

The internal radius of both sectors is kept as $R_i = D/2$, while the external radii $R_{e,1}$ and $R_{e,2}$ and angles φ_1 and φ_2 should account for the perimeter P and surface area A_T of the unit cell.

Defining,

$$A_j = \tfrac{1}{2}\varphi_j(R_{e,j}^2 - R_i^2);\ j = 1,2 \tag{10}$$

$$P_j = \varphi_j R_i;\ j = 1,2 \tag{11}$$

Then,

$$A_1 + A_2 = A_T \tag{12a}$$

$$P_1 + P_2 = P\,(=\pi R_i/2) \tag{12b}$$

Considering $R_{e,1}$, $R_{e,2}$, φ_1 and φ_2 as parameters, two additional constraints, apart from (Eqs. 12a, 12b), are introduced by requiring that the model presents the same geometrical coefficient γ and β (Eqs. 4b, 4c) as the actual unit cell:

$$\ell_1^2\,A_1\,\gamma_1 + \ell_2^2\,A_2\,\gamma_2 = \ell^2\,A_T\,\gamma \tag{12c}$$

$$\ell_1^4\,A_1\,\beta_1 + \ell_2^4\,A_2\,\beta_2 = \ell^4\,A_T\,\beta \tag{12d}$$

where $\ell_j = A_j/P_j$ and the values of the parameters γ_j and β_j are obtained from the analytical solution of Eqs. (5) for a radial fin and then using Eqs. (4b) and (4c):

$$\gamma_j = \frac{\sigma_j}{(1-\sigma_j)^3}\left[\frac{\sigma_j}{2}(4-\sigma_j) - \ln\sigma_j - \frac{3}{2}\right] \tag{13a}$$

$$\beta_j = \frac{\sigma_j^2}{(1-\sigma_j)^5}\left[(3-2\sigma_j)\ln\sigma_j + \ln^2\sigma_j - \frac{\sigma_j}{6}(30 - 15\sigma_j + 2\sigma_j^2) + \frac{17}{6}\right] \tag{13b}$$

where j = 1, 2, $\sigma_j = (R_i/R_{e,j})^2$

Finally, the fin efficiency for the 1D-TERF model can be calculated as:

$$\eta_{1D-TERF} = \frac{A_1\eta_1 + A_2\eta_2}{A_T} \tag{14}$$

where η_1 and η_2 are obtained using expression (8).

Eqs. (12a–d) allows the 1D-TERF model to match the same truncated series (4a) as the actual fin.

To carry out the solution of Eqs. (12a–d) it is convenient to work with two unknowns, say φ_1 and σ_1. Values of φ_2 and σ_2 are explicitly obtained from Eqs. (12a,b), and then Eqs. (12c,d) are used simultaneously to close the system. For all conditions tested in this work initial values $\varphi_1 = 0$ and $\sigma_1 = 1$ proved to be suitable to obtain convergence when the subroutine *Fsolved* of Matlab was used. Also, it has been checked that Eqs. (12c,d) only admit a single solution.

Values of the angle $\varphi_1/(\pi/2)$ and σ_1 for in-line and staggered layouts and different pitches are reported in Tables B5 and B6 of Appendix B.

3.3. Sector method (SECT)

In the sector method, originally suggested by Carrier and Anderson [3], the actual unit cell is divided into a finite number (n) of sectors as it is sketched in Fig. 3. Then, each sector j is replaced by an annular circular sector with the same subtended angle α_j, internal radius $R_i = D/2$ and external radius $R_{e,j}$ chosen to match the same surface area A_j of the actual sector:

$$R_{e,j} = \sqrt{\frac{4\,n\,A_j}{\pi} + (D/2)^2} \tag{15}$$

The fin efficiency (η_{SECT}) is obtained as:

$$\eta_{SECT} = \frac{\sum_{j=1}^{n} A_j\eta_j}{A_T} \tag{16}$$

where η_j is evaluated by expression (8).

The SECT method neglects heat exchange between contiguous sectors, a fact that prevents the procedure from predicting the correct efficiency as $n \to \infty$. Nonetheless, the precision increases as n is raised. As the computational demand also increase with n (Eq. (16)), a trade-off between both features will determine a suitable value of n. Kundu and Das [15] showed that for continuous fins on circular tubes, n = 20 is enough to reach the maximum precision of the method for an in-line layout with $P_T/P_L = 1$ (square layout) and $\Phi = 0.93$. For all conditions tested in this work, as discussed in the next section, it has been checked that n = 20 provides almost the maximum precision. The reported deviations when using the SECT method, therefore, correspond to n = 20.

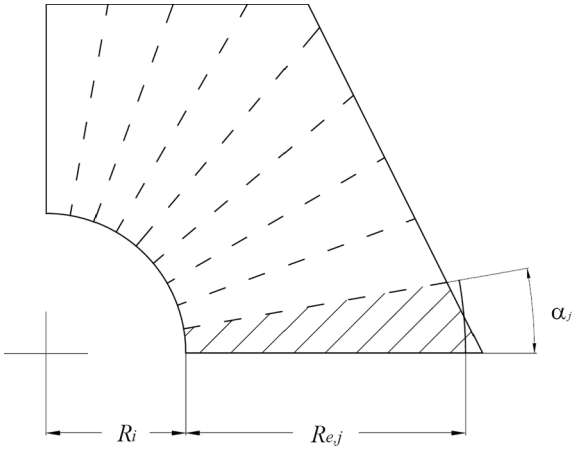

Fig. 3. Sketch for the sector method (SECT).

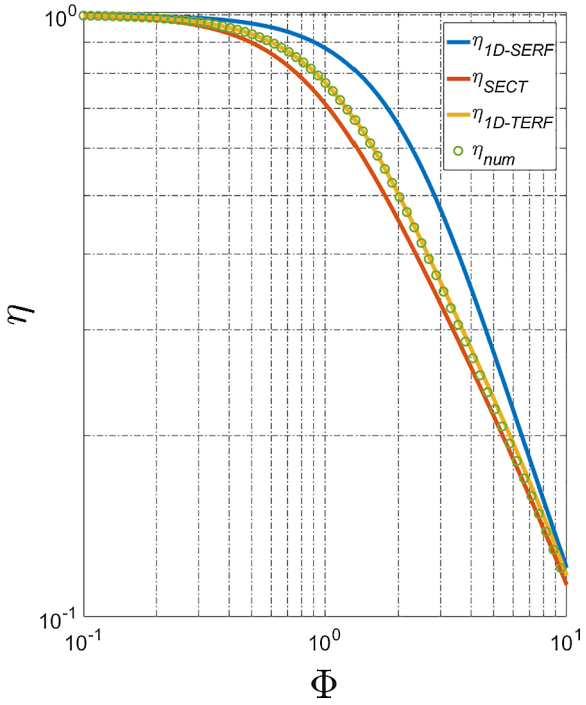

Fig. 4. η vs Φ for an in-line layout of circular tubes ($P_L = 2$ and $P_T/P_L = 2$).

4. Results and discussion

Fig. 4 shows the behavior of η as function of the fin modulus, Φ, for a continuous fin on a circular tube in an in-line layout ($P_L = 2$, $P_T/P_L = 2$). Numerical values for the actual fin, obtained employing the platform Comsol Multiphysics, and predictions from the 1D-SERF, 1D-TERF and SECT approximations are included in Fig. 4. As the limiting values are satisfied by the three approximations (*i.e.*, $\eta \to 1$ at $\Phi \to 0$ and $\eta \to 1/\Phi$ as $\Phi \to \infty$), the largest deviations arise at intermediate values of Φ.

The relative error for a given value of Φ is defined as:

$$\varepsilon_i = \frac{(\eta_i - \eta_{num})}{\eta_{num}} \cdot 100 \tag{17}$$

where η_{num} stands for the efficiency obtained from the numerical evaluation and η_i is the value provided by the approximation "i" (1D-SERF, 1D-TERF or SECT).

The accuracy of any approximation will be assessed by evaluating the maximum absolute value of ε_i as Φ is varied from 0 to ∞. Such a value, ε_i^{max}, is reported with the corresponding sign of ε_i.

Values of ε_i^{max} arising from the application of 1D-SERF, 1D-TERF and SECT methods for different P_L and P_T/P_L ratios and in-line layout are displayed in Table 1. It can be appreciated that the 1D-TERF provides the best precision in all cases. Although some of the pitch combinations in Table 1 (*e.g.*, $P_L = 1.5$ and $2 \le P_T/P_L \le 3.5$) are unlikely to be found in practice, they have been tried as an exigent test to the different approximations. Values of ε_i^{max} from the 1D-TERF model are kept below 4%, while values from the 1D-SERF and SECT methods can exceed 13% and 30% respectively.

As expected from the conception of the 1D-SERF and SECT approximations, the former over-predicts and the latter under-predicts the efficiency (Table 1).

To further explore the behavior of the different methods, Fig. 5 shows ε_i as the actual fin efficiency (η_{num}) decreases for an in-line layout with $P_L = 1.5$ and $P_T/P_L = 3.5$. The qualitative difference between the distributions of errors stems in the fact that the 1D-TERF model satisfies the truncated series of Eq. (4a) (*i.e.*, in the low range of Φ or, equivalently, in the high range of η_{num}) and the other two

Table 1
ε_i^{max} (%) arising from the prediction of η using 1D-SERF and 1D-TERF models and the sector method for in-line layout of circular tubes.

P_T/P_L	$P_L = X_L/D$											
	1.5			2.0			3.0			4.0		
↓	SERF	SECT	TERF	SERF	SECT	TERF	SERF	SECT	TERF	SERF	SECT	TERF
1.0	2.4	−1.5	−0.1	1.1	−1.3	−0.1	0.6	−1.2	−0.1	0.5	−1.1	0.0
1.5	7.2	−2.3	0.0	4.3	−2.5	−0.1	2.7	−2.7	−0.2	2.2	−2.8	−0.2
2.0	14.5	−4.2	0.5	9.6	−4.8	0.0	6.5	−5.3	−0.2	5.4	−5.6	−0.2
2.5	21.5	−6.1	1.4	15.0	−7.1	0.4	10.6	−8.0	−0.1	8.9	−8.4	−0.2
3.0	27.9	−7.9	2.5	20.2	−9.1	1.0	14.8	−10.3	0.3	12.6	−11.0	0.0
3.5	33.9	−9.6	3.8	25.1	−10.9	1.7	18.8	−12.4	0.7	16.2	−13.2	0.3

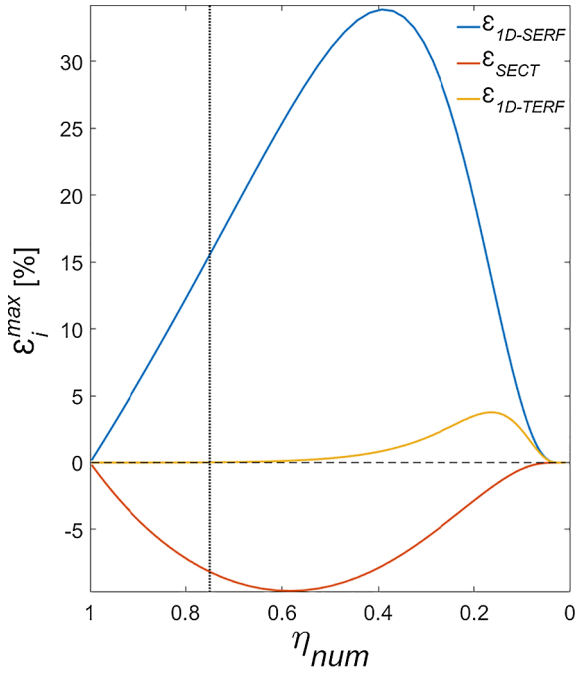

Fig. 5. ε vs. η_{num} for an in-line layout of circular tubes ($P_L = 1.5$ and $P_T/P_L = 3.5$).

approximations do not. It follows that not only the smallest error $\varepsilon_i^{max}$is produced by the 1D-TERF model, but the averaged error on the whole range of η_{num} is also much lower: 0.9% against −5.5% of the SECT method and 18.3% of the 1D-SERF model. Moreover, analyzing specifically the usual range of efficiency resulting in fin design (say, higher than 0.75), the 1D-SERF model presents errors as high as about 15%, the SECT method reaches values close −8%, while the 1D-TERF model practically do not show any significant deviation. Finally, the value ε_i^{max} takes place for the 1D-TERF model at a value of an unusual efficiency, less than 20%, a feature that is maintained for all configurations tried in the present work. It is clear that the 1D-TERF model is largely the best option to estimate the fin efficiency and thus rewards the additional effort to evaluate the shape coefficients γ and β.

Values of ε_i^{max} for staggered layouts and different combinations of pitches (*i.e.*, $1.5 \le P_L \le 4$ and $1 \le P_L/P_T \le 7$) are reported in Table 2. For this layout all the approximations present errors lower than 5% for the whole set of conditions. If that level of errors is acceptable, the 1D-SERF model is advisable due to its simplicity. If higher accuracy is required, the 1D-TERF model warranties a remarkable precision (*i.e.*, $|\varepsilon_i^{max}| \leqslant 0.2\%$) in all cases.

This fact can be best appreciated in Fig. 6, where a 3D plot of ε_i^{max} as a function of P_L and P_T/P_L is shown.

4.1. A simple approximation for high values of fin efficiency

Assuming that the coefficient γ is available for a given tube-bundle arrangement, Eq. (4a) can be used as a linear approximation in Φ^2: $\eta = 1 - \gamma\Phi^2$. However, this expression rapidly losses precision as Φ^2 increases. The following alternative equation that keeps the same initial rate of variation, $d\eta/d\Phi^2 = -\gamma$ as $\Phi^2 \to 0$ provides a much wider range of acceptable precision:

$$\eta_{high} = \frac{1}{\sqrt{1 + 2\gamma\ \Phi^2}} \tag{18}$$

Table 2
ε_i^{max} (%) arising from the prediction of η using 1D-SERF and 1D-TERF models and the sector method for staggered layout of circular tubes.

P_T/P_L	$P_L = X_L/D$											
	1.5			2.0			3.0			4.0		
↓	SERF	SECT	TERF	SERF	SECT	TERF	SERF	SECT	TERF	SERF	SECT	TERF
1.0	0.9	−0.5	0.0	0.4	−0.4	0.0	0.2	−0.4	0.0	0.2	−0.4	0.0
1.5	0.8	−0.7	−0.1	0.4	−0.7	0.0	0.3	−0.6	0.0	0.2	−0.6	0.0
2.0	1.0	−1.3	−0.1	0.7	−1.2	−0.1	0.4	−1.1	0.0	0.4	−1.1	0.0
2.5	0.6	−0.9	−0.1	0.4	−0.8	0.0	0.3	−0.8	0.0	0.2	−0.7	0.0
3.0	0.2	−0.4	0.0	0.1	−0.4	0.0	0.1	−0.3	0.0	0.1	−0.3	0.0
3.5	0.1	−0.2	0.0	0.1	−0.2	0.0	0.0	−0.2	0.0	0.0	−0.2	0.0
4.0	0.2	−0.4	0.0	0.2	−0.4	0.0	0.1	−0.4	0.0	0.1	−0.4	0.0
4.5	0.6	−0.7	0.0	0.5	−0.7	0.0	0.4	−0.7	0.0	0.3	−0.8	0.0
5.0	1.2	−1.2	−0.1	0.9	−1.3	−0.1	0.7	−1.3	−0.1	0.6	−1.3	−0.1
5.5	1.9	−1.8	−0.1	1.5	−1.9	−0.1	1.2	−1.9	−0.1	1.0	−2.0	−0.1
6.0	2.7	−2.5	−0.2	2.2	−2.6	−0.1	1.7	−2.7	−0.2	1.5	−2.7	−0.2
6.5	3.6	−3.2	−0.2	2.9	−3.3	−0.2	2.3	−3.5	−0.2	2.1	−3.5	−0.2
7.0	4.5	−3.9	−0.2	3.7	−4.1	−0.2	3.0	−4.2	−0.2	2.7	−4.4	−0.2

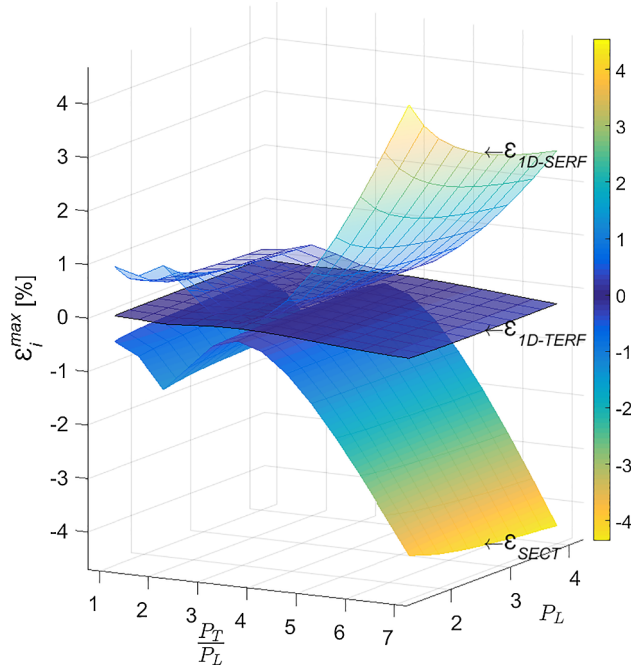

Fig. 6. ε_i^{max} vs. P_L and P_T/P_L for a staggered layout of circular tubes.

If relative deviations up to around 4% in the estimation of η are tolerated, then Eq. (18) can be used, irrespective of the tube layout, whenever the estimated value for η_{high} results higher than 0.7. Given the pitches of the tube array, in this application the value of γ can be obtained from Tables B1 or B3 of the Appendix B by a simple bilinear interpolation.

5. Conclusions

A novel one dimensional model (1D) identified as Two Radial Equivalent Fins (TERF) aiming at predicting the heat exchange rate between a fluid stream and continuous fin-and-tube devices has been presented in this contribution. In the 1D-TERF model it is proposed to replace the actual continuous fin by two radial (equivalent) fins while keeping the same surface area of the fin and the same perimeter of the tube at which the fin is attached. Thus, the dimension of the problem is reduced from 2D to 1D. The model introduces two geometrical parameters that are evaluated by matching the two first terms of the series describing the actual fin efficiency at low values of the modulus Φ ($= \ell\sqrt{h/(k\,\delta)}$). It is shown that the model thus formulated allows reaching a much better precision to estimate the efficiency of continuous fins than can be achieved using the frequently employed equivalent radial fin model and the sector method. The level of accuracy of 1D-TERF model is better than 4% for the whole set of conditions tested in this contribution covering he complete range of operative conditions (*i.e.*, the modulus Φ varying from 0 to infinity) for layouts of circular tubes presenting $4 \geq P_L \geq 1$ and $3.5 \geq P_T/P_L \geq 1$ (in-line) and $7 \geq P_T/P_L \geq 1$ (staggered).

An aspect that deserves to be highlighted is that the 1D-TERF model presents a remarkable accuracy, with almost no deviation, for the range of high to intermediate efficiencies ($\eta > 0.4$) normally found in actual design of extended surfaces, irrespective of the tube layout and pitches. In addition, if a level of error of around of 4% can be tolerated in the range of high efficiency (say $\eta > 0.7$), the simple expression (Eq. (18)) can be reliably used.

As a final aspect, it is worth to comment that the underlying concepts for the 1D-TERF model can be extended to predict efficiencies of continuous fins attached to non-circular tubes (*e.g.*, flattened or elliptical tubes).

Acknowledgments

The authors remain very thankful for the financial support of the following Argentine institutions: ANPCyT- MINCyT (PICT'16 - 3546), CONICET (PIP 0018) and UNLP (PID I226). N. J. Mariani and G. F. Barreto are research members of CONICET and F. Suárez holds a fellowship from CIC BA.

Appendix A

To perform a perturbation analysis of Eqs. (2) on Φ^2 it should be taken into account that $\theta_0 = 1$ is the solution of Eqs. (2) when $\Phi^2 = 0$. Then, an expansion of the following form can be proposed:

$$\theta = 1 + \theta_1 \Phi^2 + \theta_2 \Phi^4 + \mathcal{O}(\Phi^6) \tag{A1}$$

where the functions θ_m depend on the coordinates x^*, y^* and on the fin shape, but not on Φ^2. For convenience, it is replaced in Eq. (A1) $\theta_1 = -G/\ell^2$, $\theta_2 = B/\ell^4$:

$$\theta = 1 - (G/\ell^2)\Phi^2 + (B/\ell^4)\Phi^4 + \mathcal{O}(\Phi^6) \tag{A2}$$

By introducing Eq. (A2) into Eqs. (2) of the main text and by grouping terms of the same order in Φ^{2m},

$$\nabla^2 G = -1, \quad on \quad A_T; \tag{A3a}$$

$$G = 0, \quad on \quad \widehat{ea}; \tag{A3b}$$

$$\nabla_n G = 0, \quad on \quad ab\bar{c}de \tag{A3c}$$

$$\nabla^2 B = -G, \quad on \quad A_T; \tag{A4a}$$

$$B = 0, \quad on \quad \widehat{ea}; \tag{A4b}$$

$$\nabla_n B = 0, \quad on \quad ab\bar{c}de \tag{A4c}$$

where ∇^2 stands for the Laplace operator in the dimensional coordinates x and y. Then, employing Eq. (A2) in the definition of η, Eq. (3) in the main text:

$$\eta = 1 - \frac{\Phi^2}{\ell^2 A_T}\int_{A_T} G\,dA + \frac{\Phi^4}{\ell^4 A_T}\int_{A_T} B\,dA + \mathcal{O}(\Phi^6) \tag{A5}$$

In the following, it will be shown that $\int_{A_T} B\,dA = \int_{A_T} G^2\,dA$, a fact that avoids the solution of Eqs. (A4) in using (A5). Expressing $1 = -\nabla^2 G$(Eq.

(A3a)):

$$\int_{A_T} B\,dA = -\int_{A_T} B\,\nabla^2 G\,dA \tag{A6}$$

As $\nabla\cdot(B\,\nabla G) = \nabla B\cdot\nabla G + B\,\nabla^2 G$,

$$\int_{A_T} \nabla\cdot(B\,\nabla G)\,dA = \int_{A_T} \nabla B\cdot\nabla G\,dA + \int_{A_T} B\,\nabla^2 G\,dA \tag{A7}$$

Using the Gauss- Ostrogradsky Theorem (GOT) for the l.h.s. of Eq. (A7), defining $\Gamma = \widehat{ea}\cup ab\bar{c}de$, and considering Eqs. (A3c) and (A4b):

$$\int_{A_T} \nabla\cdot(B\,\nabla G)\,dA = \int_{\Gamma} B\,\nabla_n G\,d\Gamma = 0$$

Eq. (A7) becomes $\int_{A_T} B\,\nabla^2 G\,dA = -\int_{A_T} \nabla B\cdot\nabla G\,dA$. By replacing this result in Eq. (A6):

$$\int_{A_T} B\,dA = \int_{A_T} \nabla B\cdot\nabla G\,dA \tag{A8}$$

As $\nabla\cdot(G\,\nabla B) = \nabla B\cdot\nabla G + G\,\nabla^2 B$,

$$\int_{A_T} \nabla\cdot\ (G\,\nabla B)\,dA = \int_{A_T} \nabla B\cdot\nabla G\,dA + \int_{A_T} G\,\nabla^2 B\,dA \tag{A9}$$

Using again the GOT for the l.h.s. of Eq. (A9) and considering Eqs. (A3c) and (A4b):

$$\int_{A_T} \nabla\cdot(G\,\nabla B)\,dA = \int_{\Gamma} G\,\nabla_n B\,d\Gamma = 0$$

Eq. (A9) becomes $\int_{A_T} G\,\nabla^2 B\,dA = -\int_{A_T} \nabla B\cdot\nabla G\,dA$. By replacing this result in Eq. (A8),

$$\int_{A_T} B\,dA = -\int_{A_T} G\,\nabla^2 B\,dA \tag{A10}$$

Considering Eqs. (A4a), (A10a) can be expressed as

$$\int_{A_T} B\,dA = \int_{A_T} G^2\,dA \tag{A11}$$

Finally, by introducing Eq. (A11) into Eq. (A5), it follows that

$$\eta = 1 - \frac{\Phi^2}{\ell^2 A_T}\int_{A_T} G\,dA + \frac{\Phi^4}{\ell^4 A_T}\int_{A_T} G^2\,dA + \mathcal{O}(\Phi^6) \tag{A12}$$

Appendix B

Values of the parameters γ and β (Eqs. (4b), (c)) for the actual fin with an in-line and a staggered layout of circular tubes are included in Tables B1–B4. In addition, values of the parameters $\sigma_1 = (R_i/R_{e,1})^2$ and $F_1 = \varphi_1/(\pi/2)$ from the 1D-TERF model for the cases of in-line and staggered layout of circular tubes are reported in Tables B5 and B6, respectively.

From the values included in the set of Tables B1-B6 a simple bilinear interpolation can be performed for intermediate values of P_L and P_T/P_L. Such calculations provide a precision higher than 1% with respect to the numerical values from the solution of Eqs. (4b,c) and (12c,d).

Table B1
Values of γ (Eq. (4b)) for the actual fin with an in-line layout of circular tubes.

P_T/P_L	$P_L = X_L/D$					
↓	1.5	2.0	2.5	3.0	3.5	4.0
1.0	$2.691\cdot10^{-1}$	$1.986\cdot10^{-1}$	$1.582\cdot10^{-1}$	$1.301\cdot10^{-1}$	$1.093\cdot10^{-1}$	$9.333\cdot10^{-2}$
1.5	$2.651\cdot10^{-1}$	$1.826\cdot10^{-1}$	$1.390\cdot10^{-1}$	$1.109\cdot10^{-1}$	$9.118\cdot10^{-2}$	$7.662\cdot10^{-2}$
2.0	$2.841\cdot10^{-1}$	$1.836\cdot10^{-1}$	$1.341\cdot10^{-1}$	$1.041\cdot10^{-1}$	$8.388\cdot10^{-2}$	$6.943\cdot10^{-2}$
2.5	$2.985\cdot10^{-1}$	$1.860\cdot10^{-1}$	$1.322\cdot10^{-1}$	$1.006\cdot10^{-1}$	$7.994\cdot10^{-2}$	$6.542\cdot10^{-2}$
3.0	$3.088\cdot10^{-1}$	$1.883\cdot10^{-1}$	$1.314\cdot10^{-1}$	$9.863\cdot10^{-2}$	$7.748\cdot10^{-2}$	$6.286\cdot10^{-2}$
3.5	$3.165\cdot10^{-1}$	$1.902\cdot10^{-1}$	$1.310\cdot10^{-1}$	$9.731\cdot10^{-2}$	$7.581\cdot10^{-2}$	$6.109\cdot10^{-2}$

Table B2
Values of β (Eq. (4c)) for the actual fin with an in-line layout of circular tubes.

P_T/P_L	$P_L = X_L/D$					
↓	1.5	2.0	2.5	3.0	3.5	4.0
1.0	$8.937\cdot10^{-2}$	$4.532\cdot10^{-2}$	$2.799\cdot10^{-2}$	$1.862\cdot10^{-2}$	$1.300\cdot10^{-2}$	$9.404\cdot10^{-3}$
1.5	$8.724\cdot10^{-2}$	$3.911\cdot10^{-2}$	$2.193\cdot10^{-2}$	$1.368\cdot10^{-2}$	$9.118\cdot10^{-3}$	$6.372\cdot10^{-3}$
2.0	$1.014\cdot10^{-1}$	$4.038\cdot10^{-2}$	$2.083\cdot10^{-2}$	$1.227\cdot10^{-2}$	$7.844\cdot10^{-3}$	$5.311\cdot10^{-3}$
2.5	$1.118\cdot10^{-1}$	$4.184\cdot10^{-2}$	$2.052\cdot10^{-2}$	$1.163\cdot10^{-2}$	$7.218\cdot10^{-3}$	$4.775\cdot10^{-3}$
3.0	$1.193\cdot10^{-1}$	$4.303\cdot10^{-2}$	$2.042\cdot10^{-2}$	$1.127\cdot10^{-2}$	$6.848\cdot10^{-3}$	$4.453\cdot10^{-3}$
3.5	$1.248\cdot10^{-1}$	$4.396\cdot10^{-2}$	$2.039\cdot10^{-2}$	$1.104\cdot10^{-2}$	$6.604\cdot10^{-3}$	$4.239\cdot10^{-3}$

Table B3
Values of γ (Eq. (4b)) for the actual fin with a staggered layout of circular tubes.

P_T/P_L	$P_L = X_L/D$					
↓	1.5	2.0	2.5	3.0	3.5	4.0
1.0	$2.497 \cdot 10^{-1}$	$1.928 \cdot 10^{-1}$	$1.553 \cdot 10^{-1}$	$1.283 \cdot 10^{-1}$	$1.081 \cdot 10^{-1}$	$9.247 \cdot 10^{-2}$
1.5	$2.109 \cdot 10^{-1}$	$1.595 \cdot 10^{-1}$	$1.260 \cdot 10^{-1}$	$1.025 \cdot 10^{-1}$	$8.529 \cdot 10^{-2}$	$7.224 \cdot 10^{-2}$
2.0	$1.871 \cdot 10^{-1}$	$1.387 \cdot 10^{-1}$	$1.080 \cdot 10^{-1}$	$8.689 \cdot 10^{-2}$	$7.167 \cdot 10^{-2}$	$6.028 \cdot 10^{-2}$
2.5	$1.656 \cdot 10^{-1}$	$1.220 \cdot 10^{-1}$	$9.427 \cdot 10^{-2}$	$7.538 \cdot 10^{-2}$	$6.186 \cdot 10^{-2}$	$5.181 \cdot 10^{-2}$
3.0	$1.490 \cdot 10^{-1}$	$1.092 \cdot 10^{-1}$	$8.393 \cdot 10^{-2}$	$6.680 \cdot 10^{-2}$	$5.461 \cdot 10^{-2}$	$4.559 \cdot 10^{-2}$
3.5	$1.370 \cdot 10^{-1}$	$9.965 \cdot 10^{-2}$	$7.615 \cdot 10^{-2}$	$6.034 \cdot 10^{-2}$	$4.916 \cdot 10^{-2}$	$4.093 \cdot 10^{-2}$
4.0	$1.283 \cdot 10^{-1}$	$9.247 \cdot 10^{-2}$	$7.023 \cdot 10^{-2}$	$5.541 \cdot 10^{-2}$	$4.499 \cdot 10^{-2}$	$3.736 \cdot 10^{-2}$
4.5	$1.220 \cdot 10^{-1}$	$8.700 \cdot 10^{-2}$	$6.565 \cdot 10^{-2}$	$5.157 \cdot 10^{-2}$	$4.173 \cdot 10^{-2}$	$3.456 \cdot 10^{-2}$
5.0	$1.173 \cdot 10^{-1}$	$8.273 \cdot 10^{-2}$	$6.203 \cdot 10^{-2}$	$4.851 \cdot 10^{-2}$	$3.913 \cdot 10^{-2}$	$3.232 \cdot 10^{-2}$
5.5	$1.137 \cdot 10^{-1}$	$7.934 \cdot 10^{-2}$	$5.911 \cdot 10^{-2}$	$4.602 \cdot 10^{-2}$	$3.701 \cdot 10^{-2}$	$3.050 \cdot 10^{-2}$
6.0	$1.108 \cdot 10^{-1}$	$7.659 \cdot 10^{-2}$	$5.672 \cdot 10^{-2}$	$4.397 \cdot 10^{-2}$	$3.525 \cdot 10^{-2}$	$2.898 \cdot 10^{-2}$
6.5	$1.086 \cdot 10^{-1}$	$7.433 \cdot 10^{-2}$	$5.472 \cdot 10^{-2}$	$4.226 \cdot 10^{-2}$	$3.377 \cdot 10^{-2}$	$2.770 \cdot 10^{-2}$
7.0	$1.068 \cdot 10^{-1}$	$7.243 \cdot 10^{-2}$	$5.302 \cdot 10^{-2}$	$4.079 \cdot 10^{-2}$	$3.251 \cdot 10^{-2}$	$2.661 \cdot 10^{-2}$

Table B4
Values of β (Eq. (4c)) for the actual fin with a staggered layout of circular tubes.

P_T/P_L	$P_L = X_L/D$					
↓	1.5	2.0	2.5	3.0	3.5	4.0
1.0	$7.328 \cdot 10^{-2}$	$4.209 \cdot 10^{-2}$	$2.678 \cdot 10^{-2}$	$1.804 \cdot 10^{-2}$	$1.267 \cdot 10^{-2}$	$9.203 \cdot 10^{-3}$
1.5	$5.115 \cdot 10^{-2}$	$2.835 \cdot 10^{-2}$	$1.740 \cdot 10^{-2}$	$1.138 \cdot 10^{-2}$	$7.807 \cdot 10^{-3}$	$5.563 \cdot 10^{-3}$
2.0	$3.993 \cdot 10^{-2}$	$2.129 \cdot 10^{-2}$	$1.269 \cdot 10^{-2}$	$8.123 \cdot 10^{-3}$	$5.481 \cdot 10^{-3}$	$3.854 \cdot 10^{-3}$
2.5	$3.072 \cdot 10^{-2}$	$1.628 \cdot 10^{-2}$	$9.588 \cdot 10^{-3}$	$6.071 \cdot 10^{-3}$	$4.058 \cdot 10^{-3}$	$2.831 \cdot 10^{-3}$
3.0	$2.455 \cdot 10^{-2}$	$1.293 \cdot 10^{-2}$	$7.546 \cdot 10^{-3}$	$4.739 \cdot 10^{-3}$	$3.146 \cdot 10^{-3}$	$2.182 \cdot 10^{-3}$
3.5	$2.060 \cdot 10^{-2}$	$1.071 \cdot 10^{-2}$	$6.184 \cdot 10^{-3}$	$3.852 \cdot 10^{-3}$	$2.541 \cdot 10^{-3}$	$1.753 \cdot 10^{-3}$
4.0	$1.804 \cdot 10^{-2}$	$9.203 \cdot 10^{-3}$	$5.249 \cdot 10^{-3}$	$3.242 \cdot 10^{-3}$	$2.124 \cdot 10^{-3}$	$1.458 \cdot 10^{-3}$
4.5	$1.633 \cdot 10^{-2}$	$8.148 \cdot 10^{-3}$	$4.586 \cdot 10^{-3}$	$2.806 \cdot 10^{-3}$	$1.827 \cdot 10^{-3}$	$1.248 \cdot 10^{-3}$
5.0	$1.514 \cdot 10^{-2}$	$7.383 \cdot 10^{-3}$	$4.099 \cdot 10^{-3}$	$2.485 \cdot 10^{-3}$	$1.607 \cdot 10^{-3}$	$1.092 \cdot 10^{-3}$
5.5	$1.429 \cdot 10^{-2}$	$6.810 \cdot 10^{-3}$	$3.730 \cdot 10^{-3}$	$2.241 \cdot 10^{-3}$	$1.440 \cdot 10^{-3}$	$9.731 \cdot 10^{-4}$
6.0	$1.367 \cdot 10^{-2}$	$6.368 \cdot 10^{-3}$	$3.443 \cdot 10^{-3}$	$2.050 \cdot 10^{-3}$	$1.309 \cdot 10^{-3}$	$8.802 \cdot 10^{-4}$
6.5	$1.319 \cdot 10^{-2}$	$6.019 \cdot 10^{-3}$	$3.214 \cdot 10^{-3}$	$1.898 \cdot 10^{-3}$	$1.204 \cdot 10^{-3}$	$8.059 \cdot 10^{-4}$
7.0	$1.281 \cdot 10^{-2}$	$5.737 \cdot 10^{-3}$	$3.028 \cdot 10^{-3}$	$1.774 \cdot 10^{-3}$	$1.118 \cdot 10^{-3}$	$7.453 \cdot 10^{-4}$

Table B5
Values of σ_1 and F_1 for the 1D-TERF model (in-line layout of circular tubes).

P_T/P_L	$P_L = X_L/D$						
↓		1.5	2	2.5	3	3.5	4
1.0	σ_1	$4.642 \cdot 10^{-1}$	$3.137 \cdot 10^{-1}$	$2.327 \cdot 10^{-1}$	$1.812 \cdot 10^{-1}$	$1.458 \cdot 10^{-1}$	$1.203 \cdot 10^{-1}$
	F_1	$2.721 \cdot 10^{-1}$	$1.008 \cdot 10^{-1}$	$5.531 \cdot 10^{-2}$	$3.775 \cdot 10^{-2}$	$2.891 \cdot 10^{-2}$	$2.368 \cdot 10^{-2}$
1.5	σ_1	$4.108 \cdot 10^{-1}$	$2.570 \cdot 10^{-1}$	$1.818 \cdot 10^{-1}$	$1.375 \cdot 10^{-1}$	$1.086 \cdot 10^{-1}$	$8.838 \cdot 10^{-2}$
	F_1	$3.153 \cdot 10^{-1}$	$2.206 \cdot 10^{-1}$	$1.648 \cdot 10^{-1}$	$1.316 \cdot 10^{-1}$	$1.104 \cdot 10^{-1}$	$9.595 \cdot 10^{-2}$
2.0	σ_1	$3.739 \cdot 10^{-1}$	$2.282 \cdot 10^{-1}$	$1.576 \cdot 10^{-1}$	$1.170 \cdot 10^{-1}$	$9.108 \cdot 10^{-2}$	$7.330 \cdot 10^{-2}$
	F_1	$4.143 \cdot 10^{-1}$	$3.344 \cdot 10^{-1}$	$2.789 \cdot 10^{-1}$	$2.405 \cdot 10^{-1}$	$2.132 \cdot 10^{-1}$	$1.928 \cdot 10^{-1}$
2.5	σ_1	$3.440 \cdot 10^{-1}$	$2.068 \cdot 10^{-1}$	$1.408 \cdot 10^{-1}$	$1.032 \cdot 10^{-1}$	$7.951 \cdot 10^{-2}$	$6.346 \cdot 10^{-2}$
	F_1	$4.788 \cdot 10^{-1}$	$4.100 \cdot 10^{-1}$	$3.595 \cdot 10^{-1}$	$3.225 \cdot 10^{-1}$	$2.945 \cdot 10^{-1}$	$2.728 \cdot 10^{-1}$
3.0	σ_1	$3.184 \cdot 10^{-1}$	$1.895 \cdot 10^{-1}$	$1.276 \cdot 10^{-1}$	$9.277 \cdot 10^{-2}$	$7.094 \cdot 10^{-2}$	$5.627 \cdot 10^{-2}$
	F_1	$5.260 \cdot 10^{-1}$	$4.654 \cdot 10^{-1}$	$4.120 \cdot 10^{-1}$	$3.854 \cdot 10^{-1}$	$3.585 \cdot 10^{-1}$	$3.370 \cdot 10^{-1}$
3.5	σ_1	$2.963 \cdot 10^{-1}$	$1.750 \cdot 10^{-1}$	$1.170 \cdot 10^{-1}$	$8.444 \cdot 10^{-2}$	$6.422 \cdot 10^{-2}$	$5.070 \cdot 10^{-2}$
	F_1	$5.631 \cdot 10^{-1}$	$5.087 \cdot 10^{-1}$	$4.674 \cdot 10^{-1}$	$4.354 \cdot 10^{-1}$	$4.101 \cdot 10^{-1}$	$3.895 \cdot 10^{-1}$

Table B6
Values of σ_1 and F_1 for the 1D-TERF model (staggered layout of circular tubes).

P_T/P_L	$P_L = X_L/D$						
↓		1.5	2.0	2.5	3.0	3.5	4.0
1.0	σ_1	$4.748 \cdot 10^{-1}$	$3.167 \cdot 10^{-1}$	$2.334 \cdot 10^{-1}$	$1.813 \cdot 10^{-1}$	$1.459 \cdot 10^{-1}$	$1.204 \cdot 10^{-1}$
	F_1	$1.007 \cdot 10^{-1}$	$3.744 \cdot 10^{-2}$	$2.075 \cdot 10^{-2}$	$1.416 \cdot 10^{-2}$	$1.082 \cdot 10^{-2}$	$8.848 \cdot 10^{-3}$
1.5	σ_1	$3.494 \cdot 10^{-1}$	$2.389 \cdot 10^{-1}$	$1.761 \cdot 10^{-1}$	$1.362 \cdot 10^{-1}$	$1.090 \cdot 10^{-1}$	$9.344 \cdot 10^{-2}$
	F_1	$7.974 \cdot 10^{-2}$	$3.346 \cdot 10^{-2}$	$2.071 \cdot 10^{-2}$	$1.519 \cdot 10^{-2}$	$1.219 \cdot 10^{-2}$	$9.862 \cdot 10^{-3}$
2.0	σ_1	$2.901 \cdot 10^{-1}$	$1.966 \cdot 10^{-1}$	$1.437 \cdot 10^{-1}$	$1.104 \cdot 10^{-1}$	$8.792 \cdot 10^{-2}$	$7.191 \cdot 10^{-2}$
	F_1	$8.461 \cdot 10^{-2}$	$4.233 \cdot 10^{-2}$	$2.845 \cdot 10^{-2}$	$2.186 \cdot 10^{-2}$	$1.806 \cdot 10^{-2}$	$1.560 \cdot 10^{-2}$
2.5	σ_1	$2.492 \cdot 10^{-1}$	$1.681 \cdot 10^{-1}$	$1.224 \cdot 10^{-1}$	$9.369 \cdot 10^{-2}$	$7.439 \cdot 10^{-2}$	$6.071 \cdot 10^{-2}$
	F_1	$4.601 \cdot 10^{-2}$	$2.485 \cdot 10^{-2}$	$1.738 \cdot 10^{-2}$	$1.368 \cdot 10^{-2}$	$1.149 \cdot 10^{-2}$	$1.004 \cdot 10^{-2}$
3.0	σ_1	$2.242 \cdot 10^{-1}$	$1.506 \cdot 10^{-1}$	$1.092 \cdot 10^{-1}$	$8.337 \cdot 10^{-2}$	$6.605 \cdot 10^{-2}$	$5.381 \cdot 10^{-2}$
	F_1	$1.421 \cdot 10^{-2}$	$8.168 \cdot 10^{-3}$	$5.901 \cdot 10^{-3}$	$4.736 \cdot 10^{-3}$	$4.029 \cdot 10^{-3}$	$3.553 \cdot 10^{-3}$
3.5	σ_1	$2.181 \cdot 10^{-1}$	$1.455 \cdot 10^{-1}$	$1.050 \cdot 10^{-1}$	$7.987 \cdot 10^{-2}$	$6.308 \cdot 10^{-2}$	$5.127 \cdot 10^{-2}$
	F_1	$4.073 \cdot 10^{-3}$	$2.529 \cdot 10^{-3}$	$1.901 \cdot 10^{-3}$	$1.563 \cdot 10^{-3}$	$1.351 \cdot 10^{-3}$	$1.205 \cdot 10^{-3}$
4.0	σ_1	$1.813 \cdot 10^{-1}$	$1.204 \cdot 10^{-1}$	$8.670 \cdot 10^{-2}$	$6.587 \cdot 10^{-2}$	$5.628 \cdot 10^{-2}$	$4.530 \cdot 10^{-2}$
	F_1	$1.416 \cdot 10^{-2}$	$8.848 \cdot 10^{-3}$	$6.649 \cdot 10^{-3}$	$5.461 \cdot 10^{-3}$	$4.427 \cdot 10^{-3}$	$3.992 \cdot 10^{-3}$
4.5	σ_1	$1.641 \cdot 10^{-1}$	$1.081 \cdot 10^{-1}$	$7.755 \cdot 10^{-2}$	$5.876 \cdot 10^{-2}$	$4.628 \cdot 10^{-2}$	$3.754 \cdot 10^{-2}$
	F_1	$3.761 \cdot 10^{-2}$	$2.441 \cdot 10^{-2}$	$1.865 \cdot 10^{-2}$	$1.546 \cdot 10^{-2}$	$1.343 \cdot 10^{-2}$	$1.203 \cdot 10^{-2}$
5.0	σ_1	$1.530 \cdot 10^{-1}$	$9.998 \cdot 10^{-2}$	$7.135 \cdot 10^{-2}$	$5.388 \cdot 10^{-2}$	$4.235 \cdot 10^{-2}$	$3.428 \cdot 10^{-2}$
	F_1	$6.755 \cdot 10^{-2}$	$4.575 \cdot 10^{-2}$	$3.567 \cdot 10^{-2}$	$2.992 \cdot 10^{-2}$	$2.620 \cdot 10^{-2}$	$2.358 \cdot 10^{-2}$
5.5	σ_1	$1.444 \cdot 10^{-1}$	$9.359 \cdot 10^{-2}$	$6.646 \cdot 10^{-2}$	$5.002 \cdot 10^{-2}$	$3.921 \cdot 10^{-2}$	$3.303 \cdot 10^{-2}$
	F_1	$9.952 \cdot 10^{-2}$	$7.011 \cdot 10^{-2}$	$5.573 \cdot 10^{-2}$	$4.729 \cdot 10^{-2}$	$4.173 \cdot 10^{-2}$	$3.669 \cdot 10^{-2}$
6.0	σ_1	$1.373 \cdot 10^{-1}$	$8.830 \cdot 10^{-2}$	$6.240 \cdot 10^{-2}$	$4.889 \cdot 10^{-2}$	$3.661 \cdot 10^{-2}$	$3.053 \cdot 10^{-2}$
	F_1	$1.312 \cdot 10^{-1}$	$9.562 \cdot 10^{-2}$	$7.739 \cdot 10^{-2}$	$6.418 \cdot 10^{-2}$	$5.900 \cdot 10^{-2}$	$5.249 \cdot 10^{-2}$
6.5	σ_1	$1.313 \cdot 10^{-1}$	$8.379 \cdot 10^{-2}$	$5.894 \cdot 10^{-2}$	$4.407 \cdot 10^{-2}$	$3.439 \cdot 10^{-2}$	$2.768 \cdot 10^{-2}$
	F_1	$1.614 \cdot 10^{-1}$	$1.211 \cdot 10^{-1}$	$9.964 \cdot 10^{-2}$	$8.633 \cdot 10^{-2}$	$7.726 \cdot 10^{-2}$	$7.065 \cdot 10^{-2}$
7.0	σ_1	$1.260 \cdot 10^{-1}$	$7.987 \cdot 10^{-2}$	$5.593 \cdot 10^{-2}$	$4.170 \cdot 10^{-2}$	$3.246 \cdot 10^{-2}$	$2.608 \cdot 10^{-2}$
	F_1	$1.897 \cdot 10^{-1}$	$1.460 \cdot 10^{-1}$	$1.219 \cdot 10^{-1}$	$1.065 \cdot 10^{-1}$	$9.595 \cdot 10^{-2}$	$8.816 \cdot 10^{-2}$

Appendix C. Supplementary material

Supplementary data to this article can be found online at https://doi.org/10.1016/j.applthermaleng.2018.12.125.

References

[1] A. Aziz, A.D. Kraus, Transient heat transfer in extended surfaces, Appl. Mech. Rev. 48–7 (1995) 317–350, https://doi.org/10.1115/1.3005105.
[2] A. Campo, A.M. Delgado-Torres, Approximate, analytical procedure for rectangular annular fins by accommodating the Cauchy-Euler equation, Int. J. Heat Mass Transfer 124 (2018) 74–82, https://doi.org/10.1016/j.ijheatmasstransfer.2018.03.020.
[3] W.H. Carrier, S.W. Anderson, The resistance to heat flow through finned tubing, Heat. Piping Air Condition. 16 (1944) 304–320.
[4] H.T. Chen, J.T. Liou, Optimum dimensions of the continuous plate fin for various tube arrays, Num. Heat Transfer-Part A 34 (1998) 151–167, https://doi.org/10.1080/10407789808913983.
[5] M. Danish, S. Kumar, S. Kumar, Analysis of a nonlinear model of heat transfer through a rectangular fin: exact solutions and their multiplicity, Chem. Prod. Process Modeling 12–3 (2016) 1–17, https://doi.org/10.1515/cppm-2016-0039.
[6] R. Das, B. Kundu, Direct and inverse approaches for analysis and optimization of fins under sensible and latent heat load, Int. J. Heat Mass Transfer 124 (2018) 331–343, https://doi.org/10.1016/j.ijheatmasstransfer.2018.03.059.
[7] F. Frass, Principles of Finned-Tube Heat Exchanger Design for Enhanced Heat Transfer, second ed., WSEAS Press, 2015.
[8] S.A. Hazarika, D. Bhanja, S. Nath, B. Kundu, Thermal design parameters of a wet T-shaped fin for linear variation of humidity ratio with saturation temperature, J. Mech. Sci. Tech. 32 (5) (2018) 2391–2397, https://doi.org/10.1007/s12206-018-0451-y.
[9] J.E. Hesselgreaves, Compact Heat Exchangers. Selection, Design and Operation, Pergamon Press, 2001.
[10] H.V. Inamdar, E.A. Groll, J.A. Weibel, S.V. Garimella, Prediction of air-side particulate fouling of HVAC&R heat exchangers, Appl. Thermal Eng. 104 (2016) 720–733, https://doi.org/10.1016/j.applthermaleng.2016.05.082.
[11] J.-Y. Jang, C.-N. Lin, Two-dimensional fin efficiency of plate fin-tube heat exchangers under partially and fully wet conditions, J. Therm. Sci. 11 (2002) 249–254, https://doi.org/10.1007/s11630-002-0062-9.
[12] S.D. Keegan, N.J. Mariani, O.M. Martínez, G.F. Barreto, Behaviour of smooth catalysts at high reaction rates, Chem. Eng. J. 110 (2005) 41–56, https://doi.org/10.1016/j.cej.2005.04.013.
[13] A.D. Kraus, A. Aziz, J. Welty, Extended Surface Heat Transfer, John Wiley & Sons, 2001.
[14] D.Y. Kuan, R. Aris, H.T. Davis, Estimation of fin efficiencies of regular tubes arrayed in circumferential fins, Int. J. Heat Mass Transfer 27 (1984) 148–151, https://doi.org/10.1016/0017-9310(84), 90249-7.
[15] B. Kundu, P.K. Das, Performance of symmetric polygonal fins with and without tip loss — a comparison of different methods of prediction, The Can. J. Chem. Eng. 78 (2000) 395–401, https://doi.org/10.1002/cjce.5450780216.
[16] B. Kundu, R. Das, P.A. Wankhade, K.-S. Lee, Heat transfer improvement of a wet fin under transient response with a unique design arrangement aspect, Int. J. Heat Mass Transfer 127 (2018) 1239–1251, https://doi.org/10.1016/j.ijheatmasstransfer.2018.08.110.
[17] B. Kundu, K.-S. Lee, An appropriate analysis for optimum design of wet fins based on modified 1-D and 2-D approaches, Energy Conv. Manage. 103 (2015) 814–826, https://doi.org/10.1016/j.enconman.2015.07.024.
[18] B. Kundu, K.-S. Lee, Thermal design of an orthotropic flat fin in fin-and-tube heat exchangers operating in dry and wet environments, Int. J. Heat Mass Transfer 54 (2011) 5207–5215, https://doi.org/10.1016/j.ijheatmasstransfer.2011.08.024.
[19] T. Kuppan, Heat Exchanger Design Handbook, second ed., CRC Press, Taylor & Francis Group, 2014.
[20] S.Y. Liang, T.N. Wong, G.K. Nathan, Comparison of one-dimensional and two-dimensional models for wet-surface on efficiency of a plate-fin-tube heat exchanger, Appl. Therm. Eng. 20 (2000) (2000) 941–962, https://doi.org/10.1016/S1359-4311(99), 00078-2.
[21] Y.-T. Lin, K.-C. Hsu, Y.-J. Chang, C.-C. Wang, Performance of rectangular fin in wet conditions visualization and wet fin efficiency, J. Heat Transfer 123 (2001) 827–836, https://doi.org/10.1115/1.1391275.
[22] L. Marin, L. Elliott, P.J. Heggs, D.B. Ingham, D. Lesnic, X. Wen, Two-dimensional thermal analysis of a polygonal fin with two tubes on a square pitch, Int. J. Heat Mass Trans. 48 (2005) 3018–3033, https://doi.org/10.1016/j.ijheatmasstransfer.2004.11.030.
[23] T. Perrotin, D. Clodic, Fin efficiency calculation in enhanced fin-and-tube heat exchangers in dry conditions, Proc. 1st IIR International Congress of Refrigeration,

Washington, DC, (2003).
[24] S. Sabbaghi, A. Rezaii, Gh.R. Shahri, M.S. Baktash, Mathematical analysis for the efficiency of a semi-spherical fin with simultaneous heat and mass transfer, Int. J. Ref. 34 (2011) 1877–1882, https://doi.org/10.1016/j.ijrefrig.2011.06.014.
[25] R.K. Shah, Plate-fin and tube-fin heat exchanger design procedures, in: R.K. Shah, E.C. Subbarao, R. A. Mashelkar (Eds.), Heat Transfer Equipment Design, Hemisphere, 1988, pp. 255–266.
[26] R.K. Shah, D.P. Sekulic, Fundamentals of Heat Exchanger Design, John Wiley & Sons, Inc., 2003.
[27] K. Singh, R. Das, B. Kundu, Approximate analytical method for porous stepped fins with temperature-dependent heat transfer parameters, J. Thermophys. Heat Transfer (2016) 661–672, https://doi.org/10.2514/1.T4831.
[28] D. Taler, Basics of the Heat Exchanger Modelling (Chapter 9), Numerical Modelling and Experimental Testing of Heat Exchangers. Studies in Systems, Decision and Control, Springer, 2019, pp. 259–302.
[29] D. Taler, J. Taler, Steady state and transient heat transfer through fins of complex geometry, Arch. Thermodyn. 35–2 (2014) 117–133, https://doi.org/10.2478/aoter-2014-0017.
[30] P.A. Wankhade, B. Kundu, R. Das, Establishment of non-Fourier heat conduction model for an accurate transient thermal response in wet fins, Int. J. Heat Mass Transfer 126 (2018) 911–923, https://doi.org/10.1016/j.ijheatmasstransfer.2018.05.094.
[31] H. Zabronski, Temperature distribution and efficiency of a heat exchanger using square fins on round tubes, ASME J. Appl. Mech. 22 (1955) 119-112.
[32] G. Zhang, B. Wang, X. Lia, W. Shi, Y. Cao, Review of experimentation and modeling of heat and mass transfer performance of fin-and-tube heat exchangers with dehumidification, Appl. Therm. Eng. 146 (2019) 701–717, https://doi.org/10.1016/j.applthermaleng.2018.10.032.
[33] A. Zukauskas, Air Cooled Heat Exchangers, in: S. Kakac, A.E. Bergles, F. Mayinger (Eds.), Heat Exchangers: Thermal-Hydraulic Fundamentals and Design, Hemisphere Publication Corporation, 1981, pp. 49–83.